Effect of BSA Binding on Photophysical and Photochemical Properties of Triarylmethane Dyes

Mauricio S. Baptista and Guilherme L. Indig*

School of Pharmacy, University of Wisconsin, Madison, Wisconsin 53706

Received: February 17, 1998; In Final Form: April 14, 1998

We have employed a combination of steady-state and time-resolved spectroscopic techniques to explore the effect of protein binding on the photophysical and photochemical properties of three triarylmethane dyes: ethyl violet, crystal violet, and malachite green. Our results indicate that the binding sites of bovine serum albumin (BSA) are very efficient in preventing fast nonradiative relaxation processes that occur via rotational motion of the aromatic rings of these triarylmethanes. As a result, remarkable enhancements in fluorescence quantum yield and lifetime, intersystem crossing efficiency, and photoreactivity are observed upon protein binding. The 532 nm laser-induced photobleaching of ethyl violet noncovalently bound to BSA yields leuco ethyl violet and 4,4′-bis(diethylamino)benzophenone as reaction products. The former was more prominent in nitrogen-purged samples and the latter in air-equilibrated samples. The time-resolved transient spectra of the ethyl violet complex show superimposed elements of the spectroscopic signatures of both ethyl violet triplet and the semireduced dye radical. Based on the nature of the reaction photoproducts and transient intermediates, the first step of the bleaching process is postulated to be an electron or hydrogen atom transfer from the protein to the dye moiety. An analogous reaction mechanism was observed for protein-bound crystal violet.

Introduction

The use of photosensitizing agents and light for the treatment of neoplastic diseases, generally known as photodynamic therapy (PDT), has become a topic of increasing medical interest.[1−4] This new modality of cancer treatment has been the subject of clinical trials involving a remarkable variety of tumors, and some of the most successful procedures have already been approved by regulatory agencies of several countries.[3,4] The PDT strategy is aimed at promoting neoplastic cell death and tumor eradication through the photochemical generation of highly reactive (cytotoxic) species in situ. The combined involvement of a photosensitizer, light, and dissolved molecular oxygen has been considered as a requirement for the phototoxic effects to develop.[1−5] These oxygen-dependent deleterious effects are ordinarily designated as photodynamic action.

In a classical discussion on mechanisms of photosensitized oxidation, Foote[5] considered two categories of photoreactions that are prevalent in aerobic solutions and of essential importance for PDT. The first category takes into account processes in which the primary interaction of the electronically excited sensitizer occurs with a molecule of substrate (S). The second category describes reaction pathways in which the primary interaction involves a molecule of oxygen. Photosensitized oxidations are predominantly mediated by the first excited triplet state of the sensitizer (^{3}Sens*). Most often this occurs because the triplet lives much longer than its respective singlet, and its long lifetime favors the occurrence of the primary sensitizer−substrate and sensitizer−oxygen interactions. Long-lived triplets are especially important when considering interactions between species that are found free in solution.

The most prevalent reaction paths pertinent to biological photooxidation processes are electron or hydrogen atom transfer between the excited sensitizer and the substrate (reaction type I; eq 1) and energy transfer from the triplet sensitizer to molecular oxygen (reaction type II; eq 2).[1,5] In the photosensitization reaction type I, the radical pair formed through the primary electron or hydrogen atom transfer event can subsequently react with dissolved molecular oxygen to produce a variety of cytotoxic reactive oxygen species such as peroxyl, superoxide, and hydroxyl radicals. In the photosensitization reaction type II the reactive species formed is singlet oxygen ($^1O_2$*).

$$^3\text{Sens}^* + \text{S} \xrightarrow{k_\text{I}} \text{radical pair} \xrightarrow{O_2} \text{reactive oxygen species} \quad (1)$$

$$^3\text{Sens}^* + O_2 \xrightarrow{k_\text{II}} {}^1O_2^* \quad (2)$$

For species free in solution, the relative importance of the type I and II reactions depends on the respective reaction rates, k_I and k_II, and the concentrations of substrate and oxygen. In complex biological systems the noncovalent binding of photosensitizers to proteins, nucleic acids, and other biological substrates is likely to be a widespread phenomenon.[6−11] When the ground-state photosensitizer is physically attached to a substrate, the variables regulating the competition between reaction type I and type II are no longer those that occur for free species. The type I mechanism becomes much more competitive, especially when the excited photosensitizer is bound to a macromolecular domain that, for topological reasons, offers some protection against diffusional oxygen quenching.[12,13] The binding of photosensitizers to biopolymers has other important consequences. Within the framework of host−guest complexes the dynamics of separation of the primary photochemical

* Corresponding author: phone 608/265-6664; e-mail glindig@facstaff.wisc.edu.

S1089-5647(98)01185-7 CCC: $15.00
Published on Web 05/15/1998

products are altered, and thus reaction paths not observed for species free in solution may become more competitive in restricted reaction spaces. The photophysical and photochemical properties of photosensitizers also may be greatly affected by the nature of the microenvironment in which they are accommodated in the biopolymer,[6−11] and because diffusion no longer precedes the interaction of the excited photosensitizer with the substrate, short-lived excited singlet states are more likely to engage in the photosensitization process.

In this report we describe a study on mechanisms of photoreaction of triarylmethane dyes noncovalently bound to a model biological host (bovine serum albumin). Triarylmethane dyes are known to bind efficiently to natural and synthetic anionic biopolymer polyelectrolytes in solution[6,7,9,10] and are among the families of dyes previously considered for employment in PDT.[14,15] We are especially interested in the identification of reaction routes facilitated by the protein binding event that are distinct from oxygen-dependent type I and type II processes.

Experimental Section

Materials. Ethyl violet (EV^+, chloride salt; Aldrich), crystal violet (CV^+, chloride salt; Sigma), and malachite green (MG^+, oxalate salt; Eastman Kodak) were recrystallized from methanol, and their purity was assessed by thin-layer chromatography (TLC; silica gel, MetOH−acetic acid 95:5, v:v). Quinine sulfate monohydrate (Aldrich) was recrystallized three times from water. Potassium ferrioxalate was prepared as previously described[16] and recrystallized three times from water. Leuco ethyl violet (leuco-EV) was prepared following procedure described elsewhere[17] and recrystallized two times from 1:1 hexanes−methanol. Benzophenone was recrystallized from ethanol. Sucrose octaacetate was treated with activated carbon (Darco G-60, Aldrich) in ethanol and recrystallized two times from ethanol. All recrystallized compounds were dried under vacuum. Bovine serum albumin (BSA; initial fractionation by cold alcohol precipitation, globulin and fatty acid free) from Sigma, leuco crystal violet (leuco-CV), 4,4′-bis(dimethylamino)-benzophenone (Michler's ketone), 4,4′-bis(diethylamino)benzophenone, tetrachloro-1,4-benzoquinone, glycerol, and colloidal silica (Ludox) from Aldrich, ethyl acetate, methanol, and acetonitrile from Fisher, ethanol from Pharmco, and hexanes from EM Science were all of high-purity grade and used as supplied. Water was distilled, deionized, and filtered prior to use (Millipore Milli-Q system; resistivity, 18 MΩ cm). Unless otherwise stated, the experiments were carried out at 20 °C in 0.01 M phosphate buffer (sodium salts, from Sigma), pH 5.8 (MG^+) or pH 7.3 (EV^+ and CV^+).

Instruments and Methods. The spectrophotometric studies were performed with a Shimadzu UV-2101PC spectrophotometer. The molar extinction coefficients employed in the analytical procedures were the following ($\epsilon_{max} \times 10^{-4}$, M^{-1} cm^{-1}): in phosphate buffer, $\epsilon_{617} = 9.5$ (MG^+), $\epsilon_{595} = 9.1$ (EV^+), $\epsilon_{590} = 9.0$ (CV^+); in ethyl acetate, $\epsilon_{350} = 4.3$ (4,4′-bis(diethylamino)-benzophenone), $\epsilon_{345} = 3.9$ (Michler's ketone), $\epsilon_{273} = 5.8$ (leuco-EV), and $\epsilon_{266} = 5.6$ (leuco-CV). Fluorescence quantum yield (ϕ) and lifetime (τ_f) measurements were carried out on a Timemaster Strobemaster fluorometer from Photon Technology International, Inc. For measurement of fluorescence quantum yields, quinine sulfate in 0.5 M sulfuric acid was used as fluorescence standard ($\phi_f = 0.546$).[18,19] Fluorescence quantum yield calculations were performed using the equation[20]

$$\phi_X = \phi_R(A_R/A_X)(B_X/B_R)(I_R/I_X)(n_X/n_R)^2 \quad (3)$$

where the subscripts X and R refer to the unknown (TAM dye) and reference (quinine sulfate) samples, respectively. A is the absorbance of the sample at the wavelength of excitation, B is the integrated area under the corrected emission spectrum, I is the relative intensity of the exciting light at the wavelength of excitation, and n is the refractive index of the solution. The samples were excited at 570 nm (EV^+ and CV^+), 429 nm (MG^+), or 350 nm (quinine sulfate), and the corrected fluorescence spectra were integrated from 590 to 800 nm (TAM dyes) or from 360 to 650 nm (reference). The lifetime measurements were performed by exciting the samples at 310 nm (aqueous and glycerol solutions; N_2 filled arc lamp) or 550 nm (sucrose octaacetate glass; H_2-filled arc lamp). Fluorescence emission was detected at 90° to the excitation beam using cutoff filters (450 and 575 nm for excitation at 310 and 550 nm, respectively) to prevent scattered light from reaching the detection photomultiplier. An aqueous solution of colloidal silica was used as a standard scatterer for the acquisition of lamp profiles. The fluorescence lifetime data were analyzed using single-, double-, and triple-exponential functions, and the best fit was identified on the basis of χ^2 values, randomness of residuals, and autocorrelation function patterns.[21] The Timemaster Strobemaster software package also provided for the simultaneous analysis of several independent measurements (global data analysis).[22]

Scatchard plots[23] for the binding of EV^+ and CV^+ to BSA were obtained using fluorescence data as described elsewhere.[24] The binding constants were determined by the nonlinear fitting of the experimental data to a Langmuir type binding isotherm (eq 4),[23,25] assuming the existence of two classes of BSA binding sites for EV^+ and CV^+ (as suggested by the Scatchard analysis) and assuming that the BSA binding sites are independent, noninteracting sites.[26]

$$[Dye]_b/[BSA] = n_1K_1[Dye]_f/(1 + K_1[Dye]_f) + n_2K_2[Dye]_f/(1 + K_2[Dye]_f) \quad (4)$$

In eq 4 $[Dye]_b$ and $[Dye]_f$ are the concentrations of bound and free dye, respectively. [BSA] represents the total protein concentration, n_1 and n_2 are the number of bindings sites type 1 and 2, respectively, and K_1 and K_2 are the corresponding binding constants.

For the dye bleaching experiments the samples were placed in standard 10 mm (path length) quartz cells at a distance of approximately 10 cm from the light source. The samples were irradiated using the 532 nm line of a ND:YAG laser (Continuum model 7010) operating at 10 Hz. The defocused laser beam (circular profile with diameter of about 5 mm) was directed to the center of the quartz cell. The absolute photolysis energy was kept constant over the course of any specific experiment. The temperature-controlled cell holder allowed continuous magnetic stirring of the samples during photolysis. The photobleaching quantum efficiencies were measured considering only the first 10% decrease in dye concentration and using potassium ferrioxalate as chemical actinometer.[16,27]

Our laser flash photolysis equipment is similar to previously described systems.[28,29] The major assembly components are a nanosecond dye laser (Continuum, ND6000) pumped by a Nd:YAG laser (Continuum, 7010), used as the excitation light source, a 300 W xenon arc lamp system (Oriel, 66084), which provides the analysis beam, a monochromator (CVI, CM110), a red-sensitive photomultiplier tube (Hamamatsu, R446), and a dual-channel 600 MHz digital oscilloscope (LeCroy, 9360). Detailed description of our laser flash photolysis system will be reported elsewhere.[30]

SCHEME 1: Triarylmethane Dyes

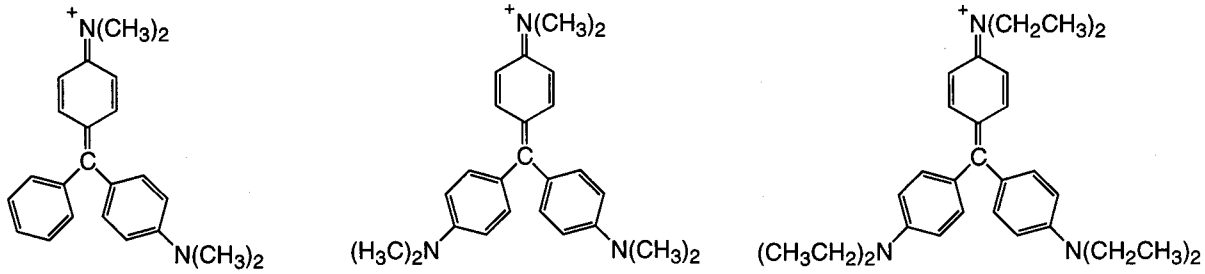

Malachite Green (MG) Crystal Violet (CV) Ethyl Violet (EV)

Qualitative analysis of low molecular weight reaction photoproducts was performed by thin-layer chromatography (TLC). The photolyzed samples were extracted with ethyl acetate (EtOAc), and the TLC analysis was run on silica gel plates (Eastman 13181, plates with fluorescence indicator) using hexanes:EtOAc 2:1 (v:v) as eluent. The photoproducts were characterized on the basis of R_F values of photolyzed and authentic (standard) samples. The observed R_F values were 0.59 ± 0.01 (Leuco-CV), 0.44 ± 0.01 (Michler's ketone), 0.65 ± 0.02 (leuco-EV), and 0.51 ± 0.02 (4,4′-bis(diethylamino)-benzophenone). MK and 4,4′-bis(diethylamino)benzophenone were detected by the inspection of the chromatogram with ultraviolet (366 nm) light. Leuco-CV and leuco-EV were visualized in their oxidized forms, CV^+ and EV^+, respectively. The oxidation of the leuco compounds on the TLC plates was performed by spraying the plates with an acetonitrile solution of tetrachloro-1,4-benzoquinone. Quantitative analysis of the reaction photoproducts was performed using UV−visible spectroscopy. The yields of the low molecular weight photoproducts were estimated on the basis of their concentration in the EtOAc extracts. Calibration curves were obtained by mixing authentic photoproducts with BSA in the same range of concentrations as was produced in the bleaching experiments and subjecting the mixture to the same process of extraction as the photolyzed samples.

Mass spectra of high molecular weight photoproducts were obtained using a matrix-assisted laser desorption/ionization (MALDI) time-of-flight (TOF) mass spectrometer (Bruker model Reflex II). After photolysis of the protein−dye samples in phosphate buffer using 532 nm laser light, the low molecular weight photoproducts were extracted from the aqueous solution with ethyl acetate, and the aqueous phase dried under a stream of nitrogen. The resulting solid was dissolved in 3 mL of water and dialyzed to infinite dilution ($>10^{10}$-fold), initially against 5% acetic acid solution and subsequently against deionized (Milli-Q) water. The protein concentration of the solutions used in the preparation of the MALDI-TOF samples was approximately 20 mM. The matrix used to facilitate sample desorption was [2-(4-hydroxyphenylazo)benzoic acid] (HABA).

Results and Discussion

I. Formation of Ground-State Complexes of BSA with TAM Dyes. We have employed a combination of photophysical techniques to characterize the formation of ground-state complexes of TAM dyes (Scheme 1) with BSA in phosphate buffer. TAM dyes show poor photoreactivity in low-viscosity media due to fast relaxation processes that occur via rotational motions of their aromatic rings.[31−33] Accordingly, in aqueous solutions the fluorescence lifetime of free TAM dyes is very short, typically in the picosecond range[31,33] (fluorescence quantum yields $\sim 10^{-5}$). In more viscous media or in microenvironments that render steric hindrance to rotational relaxation processes, fluorescence and intersystem crossing become more competitive events, and photoreactivity tends to increase.[6,7,9,10] The effect of BSA on the fluorescence of CV^+ in 0.01 M phosphate buffer at 20 °C is shown in Figure 1. The increase in CV^+ fluorescence as a function of protein concentration reaches a plateau, in agreement with the behavior expected for TAM dyes when the rigidity of the surrounding microenvironment increases.[10,33,34] At the plateau region of the binding isotherm essentially all dye molecules are noncovalently bound to the protein, thereby experiencing loss of rotational degrees of freedom. The BSA binding sites are very effective in preventing "free rotor" motions in the CV^+ moiety. This decreases the efficiency of radiationless deactivation of CV^+, a process that involves a low-lying twisted intramolecular charge-transfer state (TICT),[32] and leads to a remarkable enhancement in its fluorescence quantum yield (Table 1) and lifetime (Table 2). EV^+ shows a similar binding profile (Figure 1, inset).

For the case of MG^+, the TAM dye displaying the smallest molecular volume and largest dipole moment, the binding to BSA is less efficient. In this case, the plateau region of the binding isotherm is not reached even in the presence of BSA concentrations 2-fold higher than those required for the binding isotherms of EV^+ and CV^+ to reach a plateau (Figure 1, inset). To minimize the interference of the formation of MG^+ carbinol base during data acquisition, all studies involving MG^+ were performed at pH 5.8. At pH 7.3 the alkaline hydrolysis of MG^+ becomes more competitive, precluding the acquisition of reliable binding information. Because the flattest region of the BSA titration curve is located between pH 5 and pH 8, no significant changes in structure and charge distribution within the protein binding sites should be expected as a result of changes in pH in the 5.8−7.3 range.[35] Indeed, control experiments carried out with EV^+ and CV^+ have demonstrated that the BSA binding isotherms are analogous at both pHs (Figure 1, inset).

The effect of protein binding on the fluorescence quantum yield of EV^+ and CV^+ is similar to that observed when the viscosity[36,37] of the surrounding environment increases (at 20 °C) from 1.00 cP (water) to 1410 cP (glycerol), but not as large as what is observed when these dyes are placed in a rigid amorphous matrix (sucrose octaacetate glass; Table 1). This suggests that the steric restriction imposed by the BSA binding sites on the rotational relaxation of EV^+ and CV^+ is comparable to that experienced by these dyes in a microenvironment as cohesive as glycerol. Assuming the same sort of behavior is observed for the case of MG^+, the fluorescence quantum yield for this TAM dye bound to BSA is expected to be of the order of 3×10^{-3} (compare glycerol data in Table 1). The low

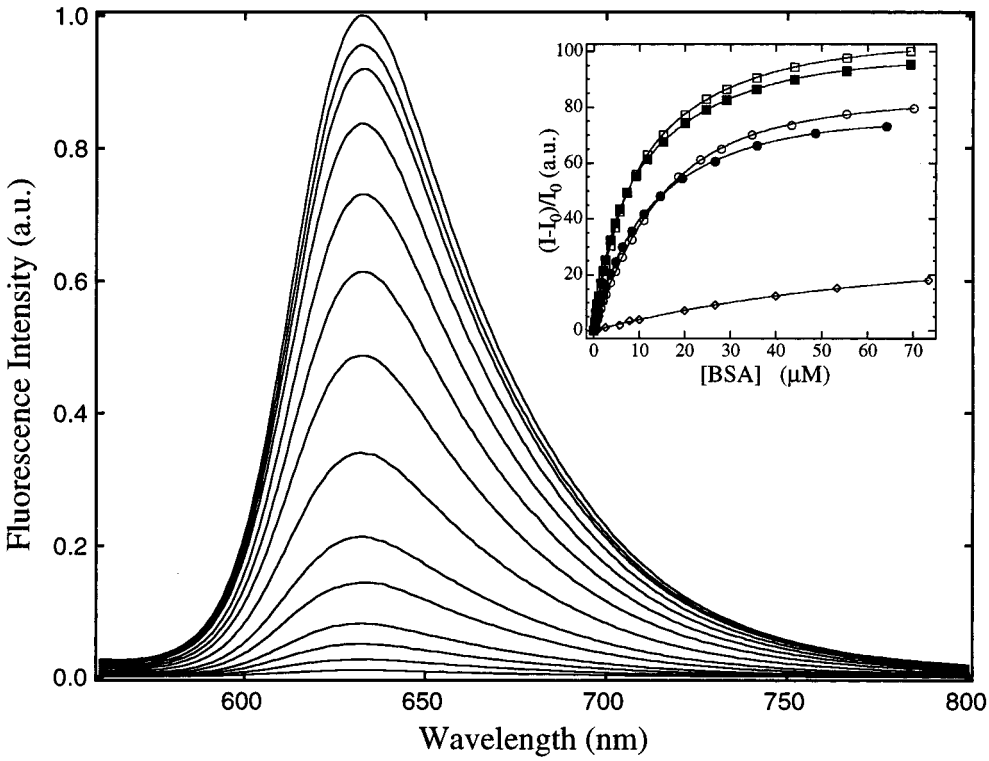

Figure 1. Effect of BSA concentration on the fluorescence spectrum of CV^+. From the bottom, in order of increasing fluorescence intensity at 632 nm, the BSA concentrations were (in μM): 0.0, 0.25, 0.62, 1.11, 2.10, 3.31, 5.68, 9.13, 13.50, 19.62, 28.79, 41.02, 49.43, and 74.67. Inset: BSA effect on the integrated fluorescence of EV^+ (squares), CV^+ (circles), and MG^+ (diamonds). Open symbols, pH 5.8; solid symbols, pH 7.3. Phosphate buffer 10 mM; [dye] = 10 μM; T = 20 °C. λ_{exc} = 520 nm (EV^+ and CV^+) or 429 nm (MG^+).

TABLE 1: Medium Effect on the Fluorescence Quantum Yield (Φ_f) of TAM Dyes

	Φ_f				
	buffer[a]	ACN	BSA[a,b]	glycerol	SOAG[c]
EV^+	9.6×10^{-5}	4.8×10^{-5}	1.7×10^{-2}	2.2×10^{-2}	0.17
CV^+	5.6×10^{-5}	3.0×10^{-5}	7.5×10^{-3}	9.2×10^{-3}	0.14
MG^+	3.7×10^{-5}	2.1×10^{-5}		3.7×10^{-3}	0.024

[a] [buffer] = 10 mM, pH 7.3 for EV^+ and CV^+ and pH 5.8 for MG^+. [b] [BSA] = 40 μM. [c] Assuming the refractive index of the sucrose octaacetate glass as 1.5.

binding efficiency of MG^+ precluded the precise assessment of its fluorescence quantum yield when bound to BSA. Also shown in Table 1 are values of fluorescence quantum yield for the TAM dyes in acetonitrile. The viscosity of acetonitrile at 20 °C is only 0.38 cP, and as expected, the fluorescence quantum yields of EV^+, CV^+, and MG^+ in acetonitrile are smaller than their respective values in aqueous solution.

The fluorescence decay of CV^+ and EV^+ bound to BSA, a typical multiple-binding-site carrier,[26,35,38] follows double-exponential functions. The global analysis of three independent determinations yielded fluorescence lifetimes of 0.4 and 2.9 ns (χ^2 = 1.032) for BSA-bound EV^+ (Table 2). For the case of BSA-bound CV^+ the respective lifetimes were 0.4 and 3.6 ns (χ^2 = 1.056). These are remarkably high values if compared with the lifetimes of CV^+ and EV^+ free in low-viscosity media (5−10 ps[31,33]). The fluorescence emission of BSA-bound MG^+ was not strong enough to permit reliable time-resolved analysis. The characterization of two populations of excited EV^+ and CV^+ might suggest the existence of two classes of binding sites for these dyes in the protein environment, and indeed, the Scatchard analysis[23,38] of EV^+ and CV^+ fluorescence data suggested the existence of two distinct BSA binding sites capable of accommodating these TAM dyes (Figure 2). The binding constants associated with the high- and low-affinity BSA binding sites were estimated via nonlinear fitting of the experimental data to Langmuir-type binding isotherms[23,25] (Figure 2, inset). The computed values of binding constants were 1.4×10^6 and 3.5×10^4 M^{-1} for the case of EV^+ and 3.4×10^5 and 2.1×10^4 M^{-1} for the case of CV^+.[39]

It is not necessarily appropriate to interpret the double-exponential fluorescence decay data by assuming the existence of two distinct BSA microenvironments that exert discrete influences on the emission properties of bound TAM molecules. Although differences in the amino acid composition or other binding site characteristic may lead to differences in the photophysical and photochemical behavior of bound TAM dyes, the fluorescence decay of EV^+ and CV^+ free in solution also follows double-exponential functions (Table 2). Therefore, it is reasonable to presume that even when bound to a single type of macromolecular binding site the fluorescence decay profiles of EV^+ and CV^+ will still typically follow double-exponential functions.

The double-exponential decay of excited singlet TAM dyes free in solution is rationalized in terms of the existence of two main populations of TAM ground-state conformers in equilibrium with each other.[40−42] Upon photoexcitation, the population of TAM molecules reaching the conformation of the TICT state faster is the one displaying the shorter fluorescence lifetime.[31] Based on the dynamics of ground-state bleach recovery, the existence of two excited singlet (S_1) TAM populations has been characterized even in low-viscosity media. For the case of CV^+ in ethanol, the ground-state bleach recovery follows double-exponential functions with decay times of 1.6 and 4.0 ps.[33]

Ground-state conformers of TAM dyes are observed in solution, owing to a peculiar characteristic of their molecular structures.[31,40−42] As consequence of steric restrictions, the aromatic rings of cationic TAM dyes are forced out of the

TABLE 2: Fluorescence Lifetimes for EV^+ and CV^+ in Several Environments[a]

	BSA[b,c]		glycerol[c]		SOAG[d]		PMAA[e]
	EV^+	CV^+	EV^+	CV^+	EV^+	CV^+	EV^+
τ_1 (ns)	0.38 ± 0.02 (0.39)	0.38 ± 0.01 (0.39)	0.32 ± 0.01 (0.33)	0.30 ± 0.01 (0.34)	0.46 ± 0.06 (0.44)	0.3 ± 0.1 (0.25)	0.5
τ_2 (ns)	3.0± 0.3 (2.9)	3.2 ± 0.4 (3.6)	4.3 ± 1.0 (4.3)	4.6 ± 0.7 (4.8)	2.76 ± 0.04 (2.70)	2.39 ± 0.09 (2.36)	2.5
f_1	0.74 ± 0.02	0.83 ± 0.05	0.86 ± 0.03	0.82 ± 0.02	0.11 ± 0.03	0.18 ± 0.04	0.63
f_2	0.26 ± 0.02	0.17 ± 0.05	0.14 ± 0.03	0.18 ± 0.02	0.89 ± 0.02	0.82 ± 0.02	0.37
χ^2	1.08 ± 0.06 (1.03)	0.97 ± 0.02 (1.06)	1.10 ± 0.05 (1.12)	1.14 ± 0.07 (1.18)	1.00 ± 0.02 (0.984)	1.01 ± 0.07 (0.991)	

[a] Values from the convoluted "best fit" of fluorescence decay curves to double-exponential functions. In parentheses are shown results of the global analysis of three to five independent measurements. [b] [BSA] = 40 mM, phosphate buffer 10 mM, pH = 7.3. [c] [Dye] = 8 μM, λ_{exc} = 310 nm. [d] Sucrose octaacetate glass; [Dye] = 6 μM, λ_{exc} = 550 nm. [e] Aqueous solution of poly(methacrylic acid), pH 3.6; data from ref 10.

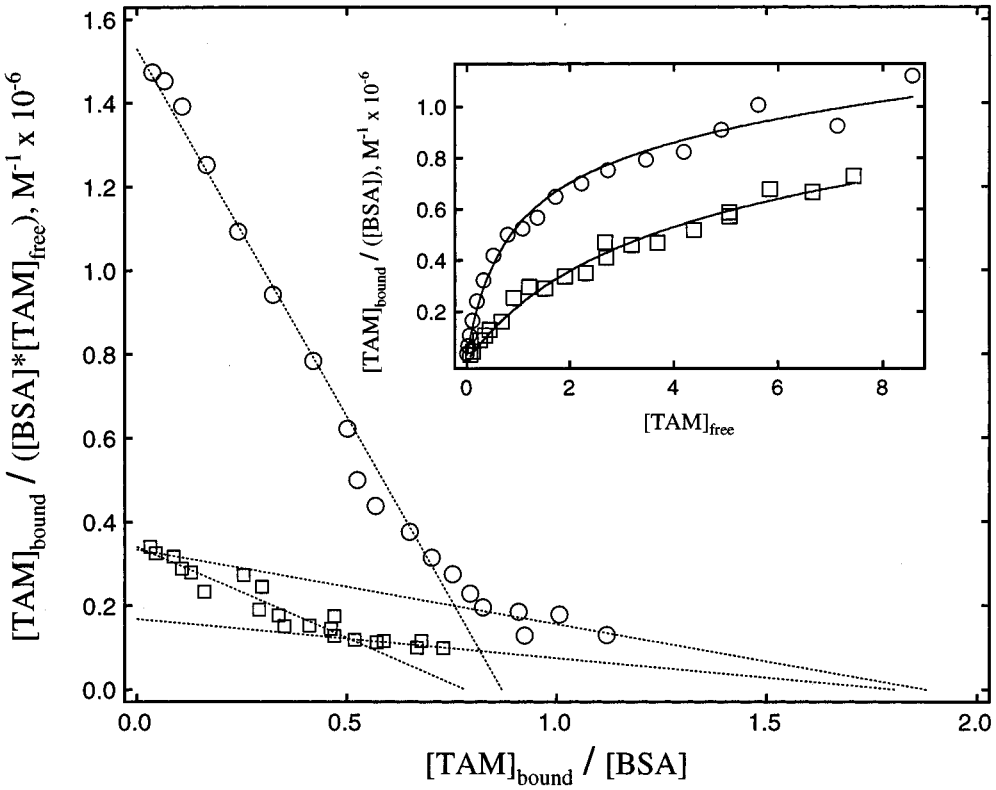

Figure 2. Scatchard plots for the binding of EV^+ (circles) and CV^+ (squares) to BSA in phosphate buffer 10 mM pH 7.3 at 20 °C. $[TAM]_b$ = concentration of dye molecules bound to BSA; $[TAM]_f$ = concentration of dye molecules free in solution, and [BSA] = total concentration of BSA (0.32 μM). The biphasic profile of the Scatchard plots suggests the existence of distinct binding sites in the BSA molecule capable of accommodating TAM molecules. The extrapolation of the dotted straight lines to the horizontal axis gives values of 0.87 and 1.88 for $EV^+$and 0.78 and 1.81 for CV^+. These values suggest the existence of two classes of BSA binding sites for these TAM molecules, each class containing only one binding site.[23,25] Inset: Langmuir-type binding isotherm. The best fit of the experimental data to eq 4 yielded the following values of binding constants: 1.4×10^6 and 3.5×10^4 M^{-1} for EV^+ and 3.4×10^5 and 2.1×10^4 M^{-1} for CV^+.

molecular plane that contains the central carbon atom. The out-of-plane angle is modulated by both the repulsion between ortho hydrogen atoms in adjacent aromatic rings and the restoration force that opposes rotation, because of the double-bond character of the twisted chemical bond. For the case of symmetric molecules, such as the triple-substituted CV^+ and EV^+, the repulsion and restorative forces acting on each distinct ring are expected to be equivalent. When the aromatic rings rotate in the same sense and the angles between them are held even, the resulting three-blade propeller is symmetric (represented by a D_3 point group), while when one of the aromatic rings rotates in the opposite sense with regard to the other two rings, an unsymmetric propeller is generated (represented by a C_2 point group). The existence of two TAM ground-state rotational isomers in equilibrium in solution was originally contemplated by Lewis and co-workers[40] as the reason for the appearance of the overlapped doublet in the absorption spectrum of CV^+.

The values of the relative integrated fluorescence intensities (*f* values; Table 2) provided by the double-exponential analysis of the fluorescence decay of EV^+ and CV^+ in glycerol and in BSA are comparable, suggesting that the population distributions of emitting species in the protein environment are similar to the respective distributions in glycerol. This is in keeping with the observation that the fluorescence quantum yields of EV^+ and CV^+ bound to BSA are comparable to their respective fluorescence yields in glycerol (Table 1). In both cases the population of excited molecules that relax faster are the ones accounting for the majority of the emitting fluorophores (respective values of relative integrated fluorescence intensities around 0.80). In glass of sucrose octaacetate, the population

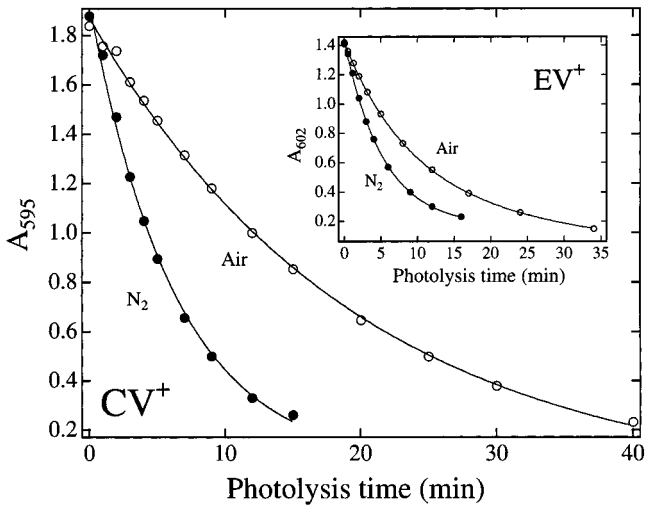

Figure 3. Effect of photolysis time on the maximum absorption of the BSA−CV^+ complex (595 nm, main panel) and the BSA−EV^+ complex (602 nm, inset). Open circles, air-equilibrated samples; solid circles, nitrogen-purged samples. Laser excitation at 532 nm, 10 Hz, 75 mJ/pulse for the CV^+ complex (50 μM BSA) and 87 mJ/pulse for the EV^+ complex (40 μM BSA). Phosphate buffer 10 mM, pH 7.3.

of emitting fluorophores displaying the longer lifetime is larger than the short-lived (subnanosecond) population, and a substantial enhancement in fluorescence quantum yield is observed for both dyes, EV^+ and CV^+.

Although fluorescence spectroscopy has been identified as a powerful technique for the detection and characterization of TAM−protein complexes, absorption spectroscopy can also provide evidence of binding. The binding of EV^+, CV^+, and MG^+ to BSA in 0.01 M phosphate buffer at 20 °C led to a small bathochromic shift in the wavelength of the maximum dye absorption. The profiles of the respective binding isotherms (λ_{max} vs [BSA]) resemble those obtained through the analysis of the protein effect on the integral fluorescence of these TAM dyes (Figure 1, inset). The wavelength of maximum MG^+ absorption is 617 nm in phosphate buffer and 621 nm in the presence of 80 μM BSA ([MG^+] = 10 μM). For the case of EV^+ the wavelength of maximum absorption shifts from 595 nm in phosphate buffer to 602 nm when bound to BSA. The respective values for CV^+ are 590 nm (buffer) and 595 nm (BSA-bound). It must be emphasized that the values shown above were obtained in the presence of a large excess of protein with respect to dye concentration. They represent spectroscopic characteristics of TAM dyes bound as monomers to BSA. Note, however, that several TAM dyes form aggregates upon binding to a variety of natural and synthetic polyelectrolytes under conditions of high polymer loading ([dye] ≫ [polymer]).[10,39,43,44] Although self-association of TAM dyes leads to remarkable increases in their photoreactivity,[10,44] this report focuses on the photophysical and photochemical properties of TAM dyes bound to the protein in their monomeric form.

II. Photochemistry of Protein−Dye Noncovalent Complexes. The observed increase in fluorescence lifetime and quantum yield of BSA-bound TAM dyes as compared to the free dyes in buffer solution suggests that the efficiency of intersystem crossing (Φ_{ISC}) might also undergo substantial increase as consequence of protein binding. We have explored the binding effect on the photochemistry of EV^+ and CV^+, the dyes thermally stable at 20 °C in phosphate buffer pH 7.3. Figure 3 shows the bleaching of BSA-bound CV^+ and EV^+ upon laser excitation at 532 nm, as measured by the decrease in absorbance at the wavelength of maximum absorption of the respective

TABLE 3: Photobleaching Efficiencies for EV^+ and CV^+ [a]

	BSA[b,c] (N_2-purged)	BSA[b,c] (air-equilibrated)	buffer[b] (air-equilibrated)
EV^+	5.5×10^{-5}	3.3×10^{-5}	2.5×10^{-6}
CV^+	3.3×10^{-5}	1.5×10^{-5}	8.4×10^{-7}

[a] Measured using potassium ferrioxalate as chemical actinometer. Photolysis carried out at 532 nm. [b] Phosphate buffer 10 mM, pH 7.3; [Dye] = 10 μM. [c] [BSA] = 40 μM.

BSA−TAM noncovalent complexes. Under photolysis conditions, essentially all TAM molecules are bound to the biopolymer (large [BSA]/[TAM] ratio; plateau region of the binding isotherms, see inset of Figure 1), thereby experiencing loss of rotational degrees of freedom. The quantum efficiency of bleaching was found to be higher in nitrogen-purged than in air-equilibrated samples (Table 3). The increased bleaching efficiency of BSA-bound EV^+ and CV^+ in nitrogen-purged samples as compared to air-equilibrated samples is an indication of the involvement of the first excited triplet state of these TAM dyes in the photobleaching process. The difference between the photobleaching efficiency of EV^+ and CV^+ free in solution and protein bound is more prominent. For the case of CV^+ an 18-fold increase is observed as a consequence of BSA binding, while for the case of EV^+ a 13-fold increase is observed (air-equilibrated samples; Table 3). Enhanced intersystem crossing (ISC) efficiency for dyes bound to macromolecules, as compared to the respective unbound dye, has been observed for a large variety of families of dyes, including triarylmethanes.[19] We were unable to detect any transient signal (nanosecond−microsecond range) following nanosecond laser excitation of EV^+ and CV^+ free in buffer solution, although well-resolved transient spectra were obtained upon excitation of these TAM dyes noncovalently bound to BSA (see below).

The analysis of low molecular weight reaction photoproducts was performed by extraction of photolyzed samples with ethyl acetate and characterization of the extracted compounds by TLC and UV−visible spectroscopy. 4,4′-Bis(diethylamino)benzophenone and leuco-EV were identified as products of laser photolysis of protein-bound EV^+. For the case of the BSA−CV^+ complex, 4,4′-bis(dimethylamino)benzophenone (Michler's ketone) and leuco-CV were characterized as photoproducts. The benzophenone-type photoproducts were more prominent in air-equilibrated samples and the leuco dyes in nitrogen-purged samples.

The reduction of a TAM dye to its leuco form is a two-electron process (formally $2e^- + H^+$ or $H + e^-$), initiated, in this case, by a photoinduced electron or hydrogen atom transfer from the protein to the dye moiety. It should be noted that 78 out of the 583 BSA amino acid residues are readily susceptible to photosensitized oxidation[5,7] (2 Trp, 4 Met, 17 His, 20 Tyr, and 35 Cys).[35,45] After initiation, and following the reaction coordinates of the bleaching process, the semireduced carbon-centered dye radical can either react with dissolved molecular oxygen to produce a benzophenone-type photoproduct or accommodate a second electron to form the leuco derivative of the TAM dye (Scheme 2). Because the electronic excitation of the dye moiety occurs within a ground-state protein−dye complex, the first excited singlet state of the dye is created physically attached to the protein. Therefore, it is conceivable that not only the TAM's triplet but also the relatively short-lived excited singlet populations may, to some extent, engage in the initial electron-transfer process that leads to the formation of the semireduced dye radical (no diffusion needed for the reaction to occur). Scheme 2 illustrates these reaction pathways.

SCHEME 2

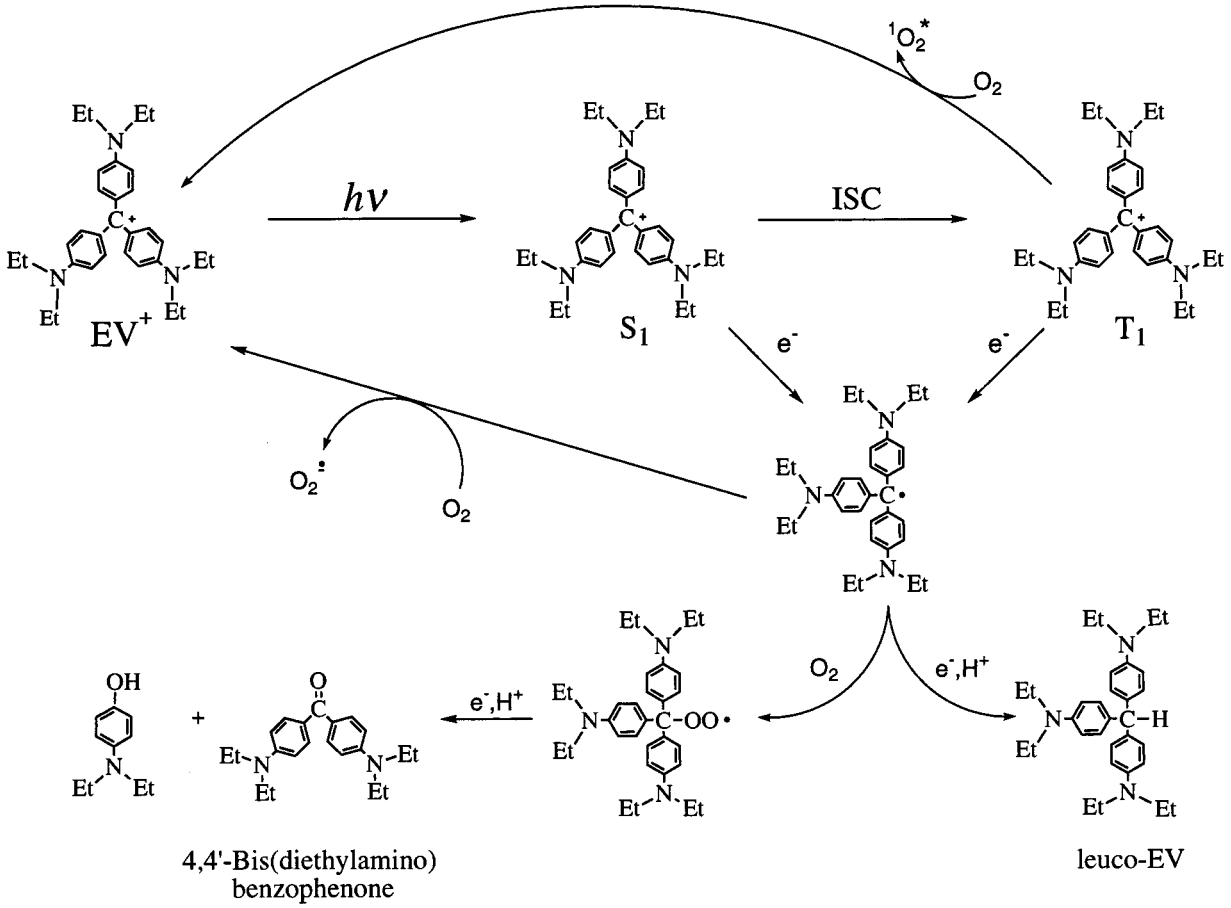

Scheme 2 also shows reaction pathways that generate singlet oxygen and superoxide radical and simultaneously preserve the photosensitizer from photodecomposition. Under aerobic conditions the collisional quenching of triplet TAM dyes by dissolved molecular oxygen prevents the triplets from engaging in the initial electron-transfer process. The singlet oxygen generated by triplet−triplet energy transfer[46] from triplet TAM to ground-state oxygen might, in principle, add to the TAM molecules to generate an unstable dioxetane intermediate whose thermal cleavage would produce benzophenone-type photoproducts. This parallel route of formation of the benzophenone-type photoproducts is, however, unlikely to play any meaningful role here.[47,48] Analogously, the oxidation of the semireduced (neutral) dye radical back to the TAM cation by molecular oxygen protects the dye from bleaching and generates another reactive oxygen species[5] as reaction product, in this case the superoxide radical.

In addition to the oxygen quenching of the TAM triplet, the oxidation of the semireduced TAM dye radical by oxygen is another reaction pathway that may contribute to the decrease in photobleaching efficiency in air-equilibrated samples as compared to nitrogen-purged samples. With the employment of spin-trapping techniques and electron paramagnetic resonance (EPR) spectroscopy, the formation of superoxide radicals during photolysis of CV^+ in air-equilibrated aqueous solutions has been observed in the presence of reducing agents such as NADH and glutathione.[49] Although the photochemical formation of singlet oxygen and superoxide radicals is of fundamental importance for the aerobic mechanisms of action of photosensitizers,[1,5] the central focus of this discussion will be kept on the mechanisms of dye photobleaching rather than emphasizing reaction routes capable of protecting the TAM dyes from photodecomposition.[50]

The competitive reaction pathways demonstrated by the characterization of reaction products in air-equilibrated and nitrogen-purged samples is also made evident through direct absorption spectroscopy measurements. Figure 4 shows that upon laser excitation of BSA-bound EV^+ in nitrogen-purged solution the photoproduct that absorbs in the 380 nm region, 4,4′-bis(diethylamino)benzophenone, is not formed in significant amounts, while the differential absorption spectrum in the 250−280 nm region clearly indicates the formation of the dye's leuco (reduced) form as photoproduct (Figure 4, inset). The BSA−CV^+ complex displayed equivalent behavior.

Control experiments have demonstrated that when CV^+ samples are photolyzed in the presence of the primary reaction photoproducts, both leuco-CV and Michler's ketone are removed from solution through secondary reaction mechanisms. The engagement of leuco-CV and Michler's ketone in secondary processes explains, at least in part, why the primary photolysis products do not fully accumulate in solution over the course of the reaction. The amounts of leuco-CV and Michler's ketone found in solution after prolonged photolysis are typically in the 10% range of the respective amount of photobleached CV^+. The samples containing EV^+ displayed analogous behavior. The low yields found for the primary low molecular weight reaction photoproducts upon prolonged photolysis may also be a consequence of the existence of competitive photodecomposition pathways leading to the formation of dye−protein heteroadducts.

The formation of dye−protein heteroadducts through the covalent linkage of dye radical intermediates with BSA was investigated with the employment of matrix-assisted laser

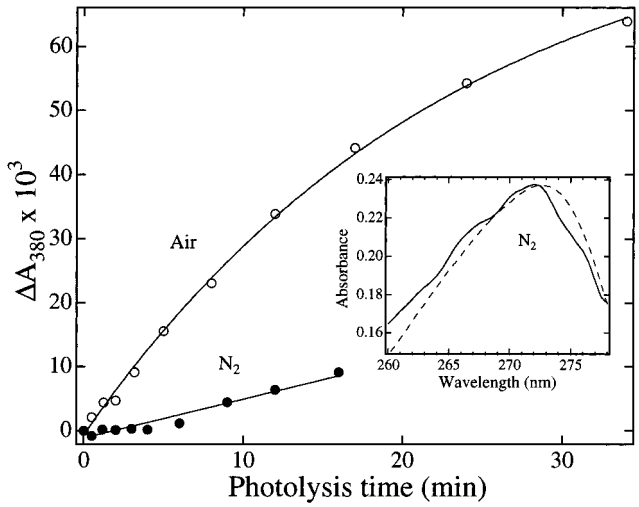

Figure 4. Changes in absorption at 380 nm upon photolysis of EV^+ noncovalently bound to BSA. The samples are the same as shown in the inset of Figure 3. The 4,4-bis(diethylamino)benzophenone is the identified reaction product which absorbs in the 380 nm region. Inset: differential spectrum obtained after 16 min of photolysis of the nitrogen-purged sample, i.e., the spectrum recorded at $t = 16$ min minus the spectrum recorded at $t = 0$ (solid line), and the absorption spectrum of leuco-EV in ethanol (dashed line).

TABLE 4: MALDI-TOF-MS Data for BSA and BSA−TAM Complexes Photolyzed at 532 nm[a]

	m/*z*, Da		
sample[b]	peak 1	peak 2	peak 3
BSA (air)	66 448		
BSA−EV^+ (air)	67 076	58 238	8520
BSA−EV^+ (N_2)	67 210	59 319	8427
BSA−CV^+ (air)	66 997	58 595	8543
BSA−CV^+ (N_2)	67 065	58 831	8575
BSA−CV^+ (N_2)	66 986	58 392	8643

[a] Values of *m*/*z* for monocharged species. [b] Air, air-equilibrated samples; N_2, nitrogen-purged samples. Samples photolyzed in the presence of phosphate buffer 10 mM, pH 7.3.

desorption/ionization time-of-flight mass spectrometry (MALDI-TOF-MS).[51−53] Samples with essentially all dye molecules bound to BSA with 1:1 stoichiometry were photolyzed to probe whether dye−protein heteroadducts are formed as a consequence of phototransformation of BSA−EV^+ and BSA−CV^+ noncovalent complexes. An increase in the mass of the protein peak was observed upon photolysis of TAM−BSA complexes in both air-equilibrated and nitrogen-purged samples (Table 4). The shift of the BSA peak is an indication of the photochemical formation of heteroadducts between BSA and the TAM dyes. The measured increases in BSA mass were slightly higher than those expect for the formation of 1:1 BSA:TAM heteroadducts. The average mass excess (0.22 kDa) is essentially identical to the mass of HABA (FW 242.23), the matrix material used to facilitate sample desorption. The formation of covalent adducts between proteins and the matrix material is an event known to interfere in MALDI-TOF-MS resolution.[53]

The mass spectrometry data also show that the laser photolysis of BSA−TAM noncovalent complexes induces the fragmentation of the biopolymer. The mass of the smaller fragmentation product is approximately 8.5 kDa (Table 4). If we assume that this smaller fragment represents a polypeptide covalently linked to a TAM molecule, then the mass of the polypeptide itself is approximately 8.1 kDa. Interestingly, by adding up the molecular weight of the amino acids of the BSA primary structure starting from its amino terminus, the amino acid sequence observed when a molecular weight between 7.9 and 8.7 kDa is reached is Gly-Cys-Glu-Lys-Ser-Leu-His.[35] This sequence contains two amino acid residues readily susceptible to photosensitized oxidation,[5,7] Cys62 (8.1 kDa peptide) and His67 (8.7 kDa peptide). The oxidative transformation of histidine residues has been identified as the primary cause of deactivation of a variety of enzymes.[5] A similar computation starting at the BSA carboxy terminus give the amino acid sequence Ile-Gln-Lys-Gly-Thr-Asp-Pro. We hypothesize that the BSA fragmentation occurs at least predominantly at the Cys62 and or His67 amino acid residues, because the 7.9−8.7 kDa amino acid sequence from the BSA carboxy terminus does not contain any amino acid residues readily susceptible to photosensitized oxidation.

Laser flash photolysis experiments provided information on the nature and spectral signatures of reaction intermediates. The time-resolved transient spectra following laser photolysis of the BSA−EV^+ noncovalent complex in air-equilibrated and nitrogen-purged samples are presented in Figure 5. In both cases the appearance of a broad transient absorption band in the 320−520 nm spectral region with a maximum around 410 nm correlates with the bleaching of ground-state EV^+. At early times after the laser pulse, the absorption maximum around 410 nm is slightly more prominent in air-equilibrated samples as compared to nitrogen-purged samples. In this last case a broader absorption envelop is observed initially, with the 410 nm peak becoming more noticeable at ca. 100 ns after the laser pulse. For wavelengths longer than 620 nm significant values of optical densities are observed only in the submicrosecond time domain. This fast component of the transient spectra with absorption beyond 620 nm also contributes to the broad absorption profile observed in the 320−520 nm region in the submicrosecond range (Figure 5). The decay of the BSA-bound EV^+ transients follow triple-exponential decay functions. The average lifetimes obtained for nitrogen-purged samples were approximately 0.04, 5, and 140 μs. Only the species displaying the longer lifetime was efficiently quenched by oxygen in the protein environment. In air-equilibrated samples the lifetime of this species was approximately 50 μs. A more rigorous analysis of the transient data to include population distributions was precluded by the weak spectroscopic signals characteristic of the systems under consideration and wide distribution of lifetimes.

Because the 320−520 nm spectral range represents a window between intense absorption bands in the EV^+ ground-state absorption spectrum, it is not surprising that EV^+ transients are repeatedly observed in this spectral region. Accordingly, following subpicosecond 606 nm excitation of EV^+ in organic solvents, the rise and decay of a picosecond (singlet) transient was noticed in the 320−520 nm region.[54] The 320−520 nm spectral window is also observed for the case of CV^+. The triplets of ethyl violet[10] and crystal violet,[55] as well as the $CV^{\bullet}$ [56−60] and $EV^{\bullet}$ [10] semireduced dye radicals, are all known to absorb light in the 320−520 nm region. However, the spectroscopic discrimination of EV^+ and CV^+ triplets from their respective free radicals is still a subject of some debate.[60]

To characterize more rigorously the formation of both the $EV^{\bullet}$ semireduced radical and the EV^+ triplet upon photolysis of BSA-bound EV^+ (Scheme 2), two experiments were carried out to determine the spectral fingerprints of each of these transient species individually. The spectral signature of the transient species formed upon laser photolysis of EV^+ in a sucrose octaacetate glass is shown in Figure 6. The transient spectra of EV^+ in the glassy medium show a broad absorption envelop in the 320−520 nm region and also considerable (positive) changes in absorption beyond 620 nm. The glassy

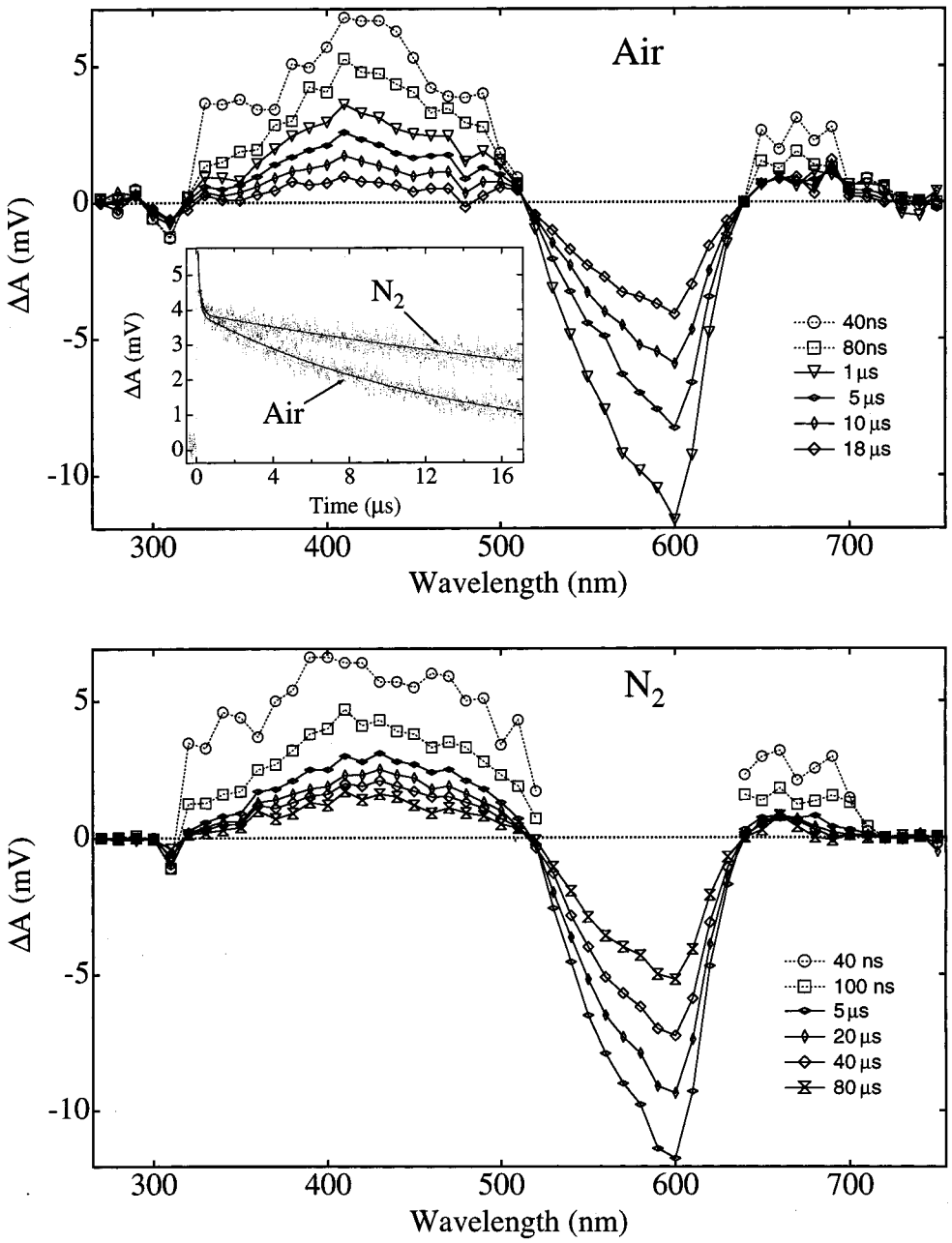

Figure 5. Transient absorption spectra of EV^+ noncovalently bound to BSA. Upper panel, air-equilibrated sample; lower panel, nitrogen-purged sample. Inset (upper panel): transient decay traces for air-equilibrated and nitrogen-purged samples recorded at 410 nm. $[EV^+] = 13\ \mu M$, [BSA] $= 40\ \mu M$, phosphate buffer 10 mM, pH 7.3, $\lambda_{exc} = 560$ nm, 108 mJ/pulse.

medium facilitates the formation of EV^+ triplets by providing a highly viscous environment, but the formation of the semireduced $EV^{\bullet}$ dye radical is minimized in this medium because sucrose octaacetate is a poor electron/H atom donor. A transient species displaying a broad absorption band in the 320−520 nm region and also displaying absorption beyond 620 nm has been observed before for EV^+ noncovalently bound to poly(methaacrylic acid) in aqueous solution and postulated as being triplet EV^+.[10] The contribution of a transient species displaying a broad absorption band in the 320−520 nm range along with significant absorption beyond 620 nm is clearly noticed in the transient spectra of BSA-bound EV^+, especially in the case of nitrogen-purged samples and at early reaction times (Figure 5).

To assess the spectral fingerprint of the semireduced $EV^{\bullet}$ radical, a mixture containing EV^+ and benzophenone in acetonitrile was photolyzed at 355 nm under conditions in which the excitation light was overwhelmingly absorbed by benzophenone. The quenching of triplet benzophenone ($^3BP^*$) by a series of triarylmethane cations, including EV^+ and CV^+, occurs at diffusion-controlled rates in acetonitrile.[60] Triplet benzophenone and other triplet carbonyls ($^3n,\pi^*$ states) are regularly quenched in solution through triplet−triplet energy-transfer processes or via electron- or hydrogen atom-transfer reactions involving molecules of solvent or other substrates present in solution.[46] The reductive electron-transfer quenching process, namely the electron or H atom transfer from a substrate to $^3BP^*$, produces the biphenyl ketyl radical ($BPH^{\bullet}$) and the corresponding electron-deficient substrate radical. The oxidative quenching of $^3BP^*$ generates the benzophenone cation radical ($BP^{\bullet+}$) and the reduced substrate radical. Oxidative quenching has been postulated as the dominant mechanism of quenching of $^3BP^*$ by CV^+ in acetonitrile.[56,59,61] As a consequence of the low viscosity of the reaction medium, a significant fraction of the initially formed $CV^{\bullet}$ and $BP^{\bullet+}$ radicals diffuse away from each

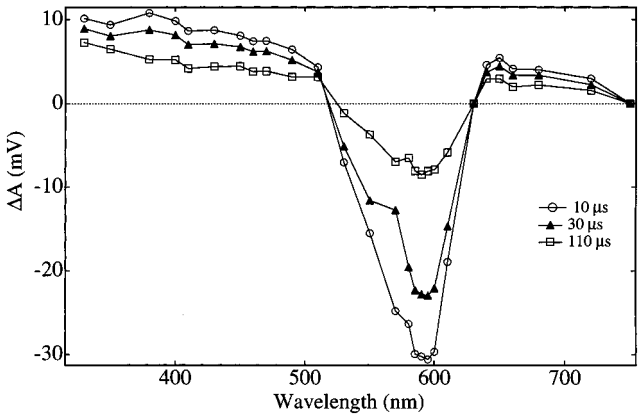

Figure 6. Transient absorption spectra for EV^+ in glass of sucrose octaacetate. $[EV^+] = 11\ \mu M$, $\lambda_{exc} = 560$ nm, 105 mJ/pulse.

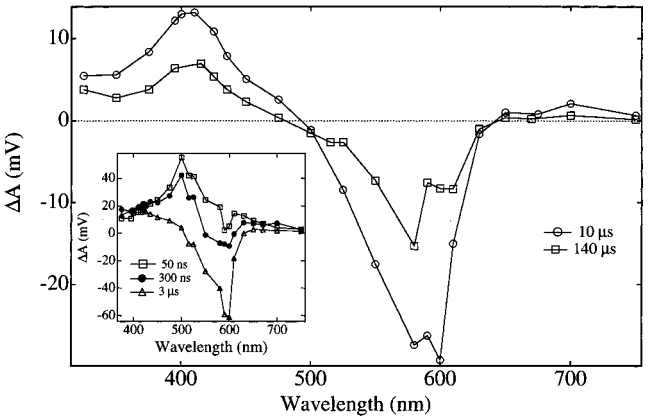

Figure 7. Transient absorption spectra for a nitrogen-purged acetonitrile solution containing BP (1.0 μM) and EV^+ (20 μM). Spectra recorded at 10 and 140 μs after the laser flash. The inset shows the respective spectra recorded at 50 ns, 300 ns, and 3 μs after the flash. $\lambda_{exc} = 355$ nm, 150 mJ/pulse.

other before the back electron transfer takes place.[61] The semireduced $CV^\bullet$ radical displays a strong bell-shaped absorption band with a maximum at 405 nm.[56] The formation of the semireduced $CV^\bullet$ radical upon laser excitation of benzophenone in BP/CV^+ mixtures in acetonitrile was confirmed by electron spin resonance spectroscopy. Upon excitation of the reaction mixture inside the resonator's cavity, the appearance of the well-known spectrum of the $CV^\bullet$ radical ($g = 2.0033$) was observed.[56]

Figure 7 shows the transient spectra obtained upon 355 nm laser excitation of a nitrogen-purged solution of benzophenone and EV^+ in acetonitrile. In the absence of benzophenone no transients were detected in the nanosecond to millisecond time domain. The decay of benzophenone triplets occur concomitantly with both the ground-state bleaching of EV^+ and the appearance of a new absorption band around 410 nm (Figure 7, inset). The EV^+ ground-state bleaching can be easily detected at short time intervals after the laser pulse, indicating that EV^+ efficiently reacts with $^3BP^*$ (see small depletion around 600 nm in the upper curve shown in the inset of Figure 7). At 10 μs after the laser pulse $^3BP^*$ no longer contributes to the observed transient spectra, and the well-defined bell-shaped absorption band with maximum around 410 nm can be attributed solely to the ethyl violet transient species. This species does not show any significant absorption beyond 620 nm. Because the spectral fingerprint of this transient is distinct from the one obtained in glass of sucrose octaacetate, we hypothesize that the transient spectra shown in Figure 7 (main panel) represents the absorption spectra of the semireduced $EV^\bullet$ radical. A virtually identical transient spectrum was observed upon reduction of triplet EV^+ with ascorbic acid, and this last spectrum is also presumed to represent the semireduced $EV^\bullet$ radical.[10] This hypothesis is supported by what has been observed for the case of CV^+ in the presence of benzophenone.[56,59]

The contribution of a species displaying absorption maximum around 410 nm is clearly observed in the transient spectra of BSA-bound EV^+ (Figure 5). Therefore, the time-resolved spectra observed upon laser photolysis of the BSA−EV^+ complex show superimposed elements of the spectroscopic signatures of both the EV^+ triplet and the semireduced $EV^\bullet$ radical. The contribution of the triplets in broadening the absorption envelop in the 320−520 nm region is more prominent at early reaction times in nitrogen-purged samples, while the contribution of the semireduced $EV^\bullet$ radical is associated with the contribution of the longer-lived species.

It is reasonable to presume that the short-lived component ($\tau \sim 40$ ns) of the broad transient signal represents a population of triplets that are efficiently quenched by electron-transfer events to generate the semireduced $EV^\bullet$ radical. Based on the MALDI-TOF-MS data, the Cys62 and His67 BSA amino acid residues were identified as the likely quenchers of this short-lived triplet population. Because the transient decay traces follow triple-exponential functions and because the longer-lived transient shows the spectroscopic characteristics of the semireduced $EV^\bullet$ radical, we hypothesize that the transient species displaying the intermediate lifetime represent a second population of EV^+ triplets, possibly bound to the second (less reactive) BSA binding site.

The time resolution of our laser flash photolysis equipment does not permit any direct inference on the involvement of EV^+ singlet populations in the formation of the semireduced $EV^\bullet$ radical. However, because the singlet population is generated while the dye is physically attached to the same protein environment that appears to be very efficient in quenching the respective triplet population, it is conceivable that semireduced $EV^\bullet$ radicals may also be produced through the reduction of the dye's singlet. At the end of the laser pulse (ca. approximately 20 ns after the flash), significant absorption around 410 nm is already observed, but whether this early population of semireduced $EV^\bullet$ radicals are formed only via efficient EV^+ triplet quenching or also through the dye's singlet manifold remains an open question.

Concluding Remarks

The formation of noncovalent complexes of TAM dyes with BSA has remarkable effects on the singlet lifetime, intersystem crossing efficiency, and photoreactivity of these photosensitizers. The laser-induced photobleaching of protein-bound triarylmethane dyes is initiated by an electron or hydrogen atom transfer from the protein to the dye moiety. The striking increase in triplet and semireduced dye radical yield caused by the binding phenomena indicates that in the presence of oxygen these photosensitizers are much more likely to engage in photosensitized oxidation processes type I and type II when bound to biopolymers than when free in solution. As suggested by the oxygen quenching effect on the longer-lived ethyl violet transient, we expect the type I process to be particularly favored in the BSA environment. When free in low-viscosity media the photoreactivity of TAM dyes is extremely poor, and no significant photodynamic action should be expected from these photosensitizers under such circumstances. Interestingly, the photochemical efficiency of BSA-bound dye bleaching increases in nitrogen-purged samples as compared to air-equilibrated

samples. Independent of the bleaching route that is dominant under anaerobic conditions (presumably, sequential two-electron abstraction from the protein or one-electron abstraction followed by the formation of protein−dye covalent adducts), upon laser excitation of protein−TAM complexes the photoinduced damage of the host protein proceeds via reaction paths that do not require oxygen to operate, and consequently are not of the ordinary photodynamic type.[5] The formation of BSA−TAM covalent adducts and BSA fragmentation represent peculiar oxygen-independent reaction courses that are well-suited for the treatment of hypoxic or poorly perfused tumor areas. The mechanistic steps of BSA-bound dye bleaching were found to be very similar between EV^+ and CV^+, suggesting that these oxygen-independent reaction paths may be rather common when considering the photochemistry of cationic photosensitizers noncovalently bound to biopolymers. TAM dyes are photosensitizers known to accumulate in the mitochondria and disrupt mitochondrial activity.[14,62] Therefore, it is likely that their phototoxicity develops upon noncovalent binding to mitochondrial proteins or other mitochondrial biopolymers. Since a large variety of families of extensively conjugated cationic dyes are known to naturally accumulate in the mitochondria,[63] as well as to bind very efficiently to natural and synthetic anionic biopolymer polyelectrolytes,[6−11] the oxygen-independent processes identified here for the case of TAM dyes are of relevance for the design of new photosensitizers specifically tailored for anaerobic phototherapy.

Acknowledgment. This work was supported by the American Cancer Society (Grant No. IRG-35-37-3) and by the Burroughs Wellcome Fund−American Foundation of Pharmaceutical Education (AACP Grant Program for New Investigators). The University of Wisconsin at Madison is also acknowledged for startup funds and continuous financial support. The authors thank Dr. T. D. Heath for editorial assistance, and Ms. J. Grant for her help with mass spectrometry measurements.

References and Notes

(1) Henderson, B. W.; Dougherty, T. J. *Photochem. Photobiol.* **1992**, *55*, 145.
(2) Levy, J. G.; Obochi, M. *Photochem. Photobiol.* **1996**, *64*, 737.
(3) Dougherty, T. J. *Photochem. Photobiol.* **1993**, *58*, 895.
(4) Kessel, D. *Drugs Today* **1996**, *32*, 385.
(5) Foote C. S. *Science* **1968**, *162*, 963.
(6) Oster, G.; Bellin, J. S. *J. Am. Chem. Soc.* **1957**, *79*, 294.
(7) Bellin, J. S.; Yankus, C. A. *Arch. Biochem. Biophys.* **1968**, *123*, 18.
(8) Yariv, S.; Ghosh, D. K.; Hepler, L. G. *J. Chem. Soc., Faraday Trans.* **1991**, *87*, 1201.
(9) Pal, M. K.; Ghosh J. K. *Spectrochim. Acta* **1994**, *50A*, 119.
(10) Jones, G. II; Oh, C.; Goswami, K. *J. Photochem. Photobiol. A: Chem.* **1991**, *57*, 65.
(11) Jones, G. II; Rahman, M. A. *J. Phys. Chem.* **1994**, *98*, 13028.
(12) Cilento, G. *Experientia* **1988**, *44*, 572.
(13) Cilento, G.; Adam, W. *Free Radicals Biol. Med.* **1995**, *19*, 103.
(14) Fiedorowicz, M.; Pituch-Noworolska, A.; Zembala, M. *Photochem. Photobiol.* **1997**, *65*, 855.
(15) Viola, A.; Hadjur, C.; Jeunet, A.; Julliard, M. *J. Photochem. Photobiol. B: Biol.* **1996**, *32*, 49.
(16) Hatchard, C. G.; Parker, C. A. *Proc. R. Soc. London, Ser. A* **1956**, *235*, 518−536.
(17) Petersen, W. C. U.S. Pat. 4,394,314, 1983.
(18) Melhuish, W. H. *J. Phys. Chem.* **1961**, *65*, 229.
(19) Meech, S. R.; Phillips, D. *J. Photochem.* **1983**, *23*, 193.
(20) Demas, J. N.; Crosby, G. A. *J. Phys. Chem.* **1971**, *75*, 991−1024.
(21) Grinvald, A.; Steinberg, I. Z. *Anal. Biochem.* **1974**, *59*, 583.
(22) Knutson, J. R.; Breechem, J. M.; Brand, L. *Chem. Phys. Lett.* **1983**, *102*, 501.
(23) Scatchard, G. *Ann. N. Y. Acad. Sci.* **1949**, *51*, 600.
(24) Naik, D. V.; Paul, W. L.; Threatte, R. M.; Schulman, S. G. *Anal. Chem.* **1975**, *47*, 267−270.
(25) Blanchard, J.; Fink, W. T.; Duffy, J. P. *J. Pharm. Sci.* **1977**, *66*, 1470.
(26) Klotz, M. L.; Huston D. L. *Trends Pharmacol. Sci.* **1988**, *4*, 253.
(27) Hamai, S.; Hirayama, F. *J. Phys. Chem.* **1983**, *87*, 83−89.
(28) Scaiano, J. C. *J. Am. Chem. Soc.* **1980**, *102*, 7747.
(29) Liao, Y.; Bohne, C. *J. Phys. Chem.* **1996**, *100*, 734.
(30) Kavalauskas, M. P.; Indig, G. L. To be published.
(31) Sundström, V.; Gillbro, T.; Bergström, H.*Chem. Phys.* **1982**, *73*, 439.
(32) Vogel, M.; Rettig, W. *Ber. Bunsen-Ges. Phys. Chem.* **1985**, *89*, 962−968.
(33) Ben-Amotz, D.; Harris, C. B. *Chem. Phys. Lett.* **1985**, *119*, 305.
(34) Kemnitz, K.; Yoshihara, K. *Chem. Lett.* **1990**, 1789.
(35) Peters, T., Jr. In *All About Albumin. Biochemistry, Genetics, and Medical Applications*; Academic Press: New York, 1996.
(36) Viswanath, D. S.; Natarajan, G. In *Data Book of the Viscosity of Liquids*; Hemisphere: New York, 1989.
(37) Gray, D. E. In *American Institute of Physics Handbook*, 3rd ed.; McGraw-Hill: New York, 1972.
(38) Das, R.; Mitra, S.; Nath, D.; Mukherjee, S. *J. Phys. Chem.* **1996**, *100*, 14514.
(39) The formation of dye aggregates under conditions of high BSA loading ([TAM] ≫ [BSA]) may also contribute to the biphasic character of the Scatchard plots. However, the spectral evidence for the formation of dye aggregates is extremely faint, even when considering the highest BSA loading employed in this analysis. Under conditions of high [TAM]/[BSA] ratios the most pronounced changes in the TAM's absorption spectra induced by BSA binding are observed in the $A_{max}/A_{shoulder}$ ratio (represented by the A_{595}/A_{550} ratio in the case of EV^+). The maximum change observed in this spectral parameter over the course of the Scatchard analysis was approximately 5%, and it would be very difficult to determine unambiguously the contributions of dye aggregate formation and dye monomer−BSA complex formation, respectively, to this small change. Further discusion on this subject can be found in ref 44.
(40) Lewis, G. N.; Magel, T. T.; Lipkin, D. *J. Am. Chem. Soc.* **1942**, *64*, 1774.
(41) Ishikawa, M.; Maruyama, Y. *Chem Phys. Lett.* **1994**, *219*, 416.
(42) Maruyama, Y.; Ishikawa, M.; Satozono, H. *J. Am. Chem. Soc.* **1996**, *118*, 6257.
(43) Pal, M. K.; Ghosh, J. K. *Spectrochim. Acta* **1994**, *50A*, 119.
(44) Duxbury, D. F. *Chem. Rev.* **1993**, *93*, 381.
(45) Hirayama, N.; Akashi, S.; Furuya, M.; Fukuhara, K. *Biochem. Biophys. Res. Commun.* **1990**, *173*, 639.
(46) Gilbert, A.; Baggott, J. In *Essentials of Molecular Photochemistry*; Blackwell Publications: London, 1991.
(47) Kuramoto, N.; Kitao, T. *Dyes Pigm.* **1982**, *3*, 49.
(48) Denman, S.; Jameel, S.; Hay, J.; Sugden, J. K. *Dyes Pigm.* **1996**, *30*, 67.
(49) Fischer, V.; Harrelson, W. G., Jr.; Chignell, C. F.; Mason, R. P. *Photobiochem. Photobiophys.* **1984**, *7*, 111.
(50) The back electron transfer from the semireduced dye radical to the protein backbone is another reaction route capable of protecting the TAM dyes from photobleaching.
(51) Muddiman, D. C.; Bakhtiar, R.; Hofstadler, S. A.; Smith, R. D. *J. Chem. Educ.* **1997**, *74*, 1288.
(52) Hillenkamp, F. *Adv. Mass. Spectrom.* **1995**, *13*, 95.
(53) Weinberger, S. R. *Spectroscopy* **1992**, *7*, 54.
(54) Martin, M. M.; Plaza, P.; Meyer, Y. H. *Chem. Phys.* **1991**, *153*, 297.
(55) Jones, G. II; Goswami, K. *J. Phys. Chem.* **1986**, *90*, 5414.
(56) Jockusch, S.; Timpe, H. J.; Fischer, C.-H.; Schnabel, W. *J. Photochem. Photobiol. A: Chem.* **1992**, *63*, 217.
(57) Bhasikuttan, A. C.; Shastri, L. V.; Sapre, A. V.; Rama Rao, K. S. V.; Mittal J. P. *J. Photochem. Photobiol. A: Chem.* **1994**, *84*, 237.
(58) Bhasikuttan, A. C.; Sapre, A. V.; Rama Rao, K. S. V.; Mittal, J. P. *Photochem. Photobiol.* **1995**, *62*, 245.
(59) Jockusch, S.; Timpe, H. J.; Schnabel, W.; Turro, N. J. *J. Photochem. Photobiol. A: Chem.* **1996**, *96*, 129.
(60) Naguib, Y. M. A.; Steel, C.; Cohen, S. G.; Young, M. A. *J. Photochem. Photobiol. A: Chem.* **1996**, *96*, 149.
(61) In addition to the 3BP* oxidative quenching by CV^+, other routes of formation of the semireduced $CV^{\bullet}$ radical are likely to operate in this system. The free radicals generated upon H atom abstraction from acetonitrile or CV^+ molecules by triplet benzophenone can also promote the reduction of the crystal violet cation to its semireduced radical. Further discussion on this mechanistic route can be found in refs 56 and 57.
(62) Gadelha, F. R.; Moreno, S. N. J.; De Souza, W.; Cruz, F. S.; DoCampo, R. *Mol. Biochem. Parasitol.* **1989**, *34*, 117.
(63) Chen, L. B. *Methods Cell. Biol.* **1989**, *29*, 103.